Non-steady electro-osmotic flow of a micropolar fluid in a microchannel

2009 J. Phys. A: Math. Theor. 42 355501

(http://iopscience.iop.org/1751-8121/42/35/355501)

IOP PUBLISHING JOURNAL OF PHYSICS A: MATHEMATICAL AND THEORETICAL

J. Phys. A: Math. Theor. **42** (2009) 355501 (14pp) doi:10.1088/1751-8113/42/35/355501

Non-steady electro-osmotic flow of a micropolar fluid in a microchannel

Abuzar A Siddiqui[1] **and Akhlesh Lakhtakia**[2]

[1] Department of Basic Sciences, Bahauddin Zakariya University, Multan, Pakistan
[2] NanoMM–Nanoenginered Metamaterials Group, Department of Engineering Science and Mechanics, Pennsylvania State University, University Park, PA 16802, USA

E-mail: abidzero0@yahoo.co.uk and akhlesh@psu.edu

Received 24 April 2009, in final form 14 July 2009
Published 12 August 2009
Online at stacks.iop.org/JPhysA/42/355501

Abstract

We formulated the initial-boundary-value problem of non-steady electro-osmotic flow of a micropolar fluid in a rectangular microchannel of height much larger than the Debye length and length much larger the height. Solving the governing differential equations numerically when a spatially uniform electric field is applied as an impulse of finite magnitude, we found that the effect is instantaneous on the flow, just as for simple Newtonian fluids. The decay times of the fluid velocity and the microrotation, however, are smaller in micropolar fluids than in simple Newtonian fluids. The maximum magnitude of microrotation decreases as the micropolarity increases. The effect of microrotation on the stress tensor is more dominant than that of the fluid speed, and a threshold effect with respect to the magnitude of the zeta potential is evident in the spatial profile of the couple stress tensor. We expect similar trends even when the applied electric field varies over some finite interval of time.

PACS numbers: 47.50.−d, 47.57.E−, 47.61.−k

1. Introduction

The flows of many technoscientifically important fluids—such as blood, colloidal suspensions, liquid crystals and epoxies—cannot be described by a simple Newtonian model. Being a suspension of rigid/semi-rigid particles that not only translate but also rotate about axes passing through their centroids, such a fluid not only sustains body forces and the usual (Cauchy) stress tensor as simple Newtonian fluids do, but also sustains body couples and couple stress tensor. The stress tensor is asymmetric in such a fluid, unlike in a simple Newtonian fluid. Having six degrees of freedom—three more than a simple Newtonian fluid—a fluid of this type is called a *micropolar* fluid (Ariman *et al* 1973, Eringen 2001).

As micropolar fluids of biological provenance are used in pathological laboratories (Eringen 1973, Turk *et al* 1973, Misra and Ghosh 2001), and because there is a rapid trend towards the deployment of labs-on-a-chip (Eijkel and van den Berg 2006, Riehemann *et al* 2009), we embarked on a program to analyse the electro-osmotic flow of a micropolar fluid in a rectangular microchannel. A study of electro-osmotic flows is relevant to fluid transport in biological and chemical instruments (Fluri *et al* 1996), specifically in channels in microchips for the analysis of DNA sequences and for drug delivery (Arangoa *et al* 1999).

In the first step of our program (Siddiqui and Lakhtakia 2009), we focused on steady flows. An expression for the Helmholtz–Smoluchowski velocity (Probstein 1989, p 192) of a micropolar fluid in a uniform rectangular microchannel, under the action of a uniform applied electric field was formulated. Numerical solutions of the relevant boundary-value problem turned out to be virtually identical to the analytic solutions obtained after using the Debye–Hückel approximation (Li 2004) when applicable. For a fixed Debye length (Li 2004), the midchannel fluid speed was found to be linearly proportional to the microchannel height when the fluid is micropolar, but not when the fluid is simple Newtonian. We also found that the couple stress decreases midchannel, but the couple stress at the walls intensifies, as the microchannel height increases and the flow tends towards turbulence.

Our focus has now moved on to non-steady flow of a micropolar fluid in a uniform rectangular microchannel under the action of a spatially uniform finite-electric-field impulse, which would trigger a specific activity in a microchip. Following the predecessor paper (Siddiqui and Lakhtakia 2009), our interest lies in the spatiotemporal variations of the fluid speed, microrotation, stress tensor and couple stress tensor in the microchannel. We are also interested in a comparison with the analogous flow of a simple Newtonian fluid in a microchannel, in order to isolate the effects of micropolarity.

This paper is organized as follows: the formulation of a relevant initial-boundary-value problem is presented in section 2, while section 3 contains the description of the numerical approach that we adopted to solve that problem. Section 4 comprises numerical results obtained and discussions thereon. The main conclusions are summarized in section 5.

2. Basic analysis and formulation

Adopting the notation $\mathbf{r}' = x'\hat{\mathbf{x}} + y'\hat{\mathbf{y}} + z'\hat{\mathbf{z}}$ for the position vector, where $\{\hat{\mathbf{x}}, \hat{\mathbf{y}}, \hat{\mathbf{z}}\}$ is the triad of Cartesian unit vectors, we are interested in examining the non-steady flow of a micropolar fluid in the microchannel $|y'| \leqslant h$ for $x' \in [-w, w]$, when the length $2w$ is much greater than the height $2h$ of the microchannel, and there is no variation along the z'-axis. The walls $y' = \pm h$ are assumed to be perfectly insulating and impermeable. Furthermore, we assume that (i) neither a pressure gradient nor a body couple is present; (ii) the effect of gravity is unimportant; (iii) the flow is symmetric as both walls are identical; (iv) a spatially uniform but time-dependent electric field is applied to the fluid; (v) the Joule heating effects are small enough to be ignored, and (vi) the micropolar fluid is ionized, incompressible and viscous.

Under these conditions, the three applicable equations of micropolar-fluid flow are as follows (Eringen 2001):

$$\nabla' \cdot \mathbf{V}'(\mathbf{r}', t') = 0, \tag{1}$$

$$-(\mu + \chi)\nabla' \times [\nabla' \times \mathbf{V}'(\mathbf{r}', t')] + \chi \nabla' \times \mathbf{v}'(\mathbf{r}', t') + \rho'_e(\mathbf{r}')\mathbf{E}'_{\text{app}}(t') = \rho \frac{\mathrm{D}}{\mathrm{D}t'}\mathbf{V}'(\mathbf{r}', t'), \tag{2}$$

$$(\alpha + \beta + \gamma)\nabla'[\nabla' \cdot \mathbf{v}'(\mathbf{r}', t')] - \gamma \nabla' \times [\nabla' \times \mathbf{v}'(\mathbf{r}', t')] - 2\chi \mathbf{v}'(\mathbf{r}', t') + \chi \nabla' \times \mathbf{V}'(\mathbf{r}', t') = \rho j_o \frac{\mathrm{D}}{\mathrm{D}t'}\mathbf{v}'(\mathbf{r}', t'). \tag{3}$$

Here, $\mathrm{D}/\mathrm{D}t'$ is the material derivative; $\mathbf{V}'$, $\mathbf{v}'$ and $\mathbf{E}'_{\rm app}$ are, respectively, the fluid velocity, the microrotation and the applied electric field; ρ is the mass density whereas $j_o = 2\gamma/(2\mu+\chi)$ is the microinertia (Ahmadi 1976, p 640); μ and χ are the Newtonian shear viscosity coefficient and the vortex viscosity coefficient, respectively; and α, β and γ are the three spin-gradient viscosity coefficients. Let us note that $\mathbf{v}'$, χ, α, β and γ are null-valued in a simple Newtonian fluid.

In the absence of a significant convective or electrophoretic disturbance to the electric double layers present in the vicinities of the walls $y' = \pm h$, the charge density $\rho'_e(\mathbf{r}')$ is described by a Boltzmann distribution, and takes the following form for a symmetric, dilute and univalent electrolyte (Li 2004):

$$\rho'_e(\mathbf{r}') = -2z_o e n_o \sinh[z_o e\psi'(\mathbf{r}')/k_B T]. \tag{4}$$

Here, z_o is the absolute value of the ionic valence, ψ' is the electric potential, e is the charge of an electron, n_o is the number density of ions in the fluid far away from any charged surface, k_B is the Boltzmann constant and T is the temperature. With ϵ denoting the static permittivity of the fluid, the charge density and the electric potential are also related by the Gauss law as follows:

$$\nabla'^2\psi'(\mathbf{r}') = (2z_o e n_o/\epsilon)\sinh[z_o e\psi'(\mathbf{r}')/k_B T]. \tag{5}$$

The Debye length $\lambda_D = (z_o e)^{-1}(\epsilon k_B T/2n_o)^{1/2}$ is assumed in this paper to be much smaller than h; i.e., $\lambda_D \ll h$.

Before proceeding, let us define the non-dimensionalized quantities

$$\left.\begin{array}{ll}
\mathbf{r} = \dfrac{1}{h}\mathbf{r}', & t = \dfrac{U}{h}t' \\
\mathbf{V} = \dfrac{1}{U}\mathbf{V}', & \mathbf{v} = \dfrac{h}{U}\mathbf{v}' \\
\psi = \dfrac{1}{\psi_o}\psi', & \rho_e = \dfrac{h^2}{\epsilon\psi_o}\rho'_e \\
\mathbf{E}_{\rm app} = \dfrac{1}{E_o}\mathbf{E}'_{app}, & m_{pq} = \dfrac{h^2}{\gamma U}m'_{pq} \\
\sigma_{pq} = \dfrac{h}{(\mu+\chi)U}\sigma'_{pq} &
\end{array}\right\}. \tag{6}$$

Here m'_{pq} and σ'_{pq} are, respectively, components of the couple stress and the (Cauchy) stress tensors, where $p, q \in \{1, 2, 3\}$;

$$U = -\frac{\epsilon\psi_o E_o}{\mu+\chi} \tag{7}$$

is a characteristic speed (Siddiqui and Lakhtakia 2009); $E_o \geqslant 0$ is a reference value of the magnitude of the applied electric field to be prescribed later and ψ_o is called the zeta potential (Li 2004) which is assumed to be temporally constant and spatially uniform at the walls $y = \pm 1$. With these quantities, equations (1)–(3) and (5), respectively, simplify to

$$\nabla\cdot\mathbf{V}(\mathbf{r},t) = 0, \tag{8}$$

$$-\nabla\times[\nabla\times\mathbf{V}(\mathbf{r},t)] + k_1\nabla\times\mathbf{v}(\mathbf{r},t) + \rho_e(\mathbf{r})\mathbf{E}_{\rm app}(t) = R_e\frac{\mathrm{D}}{\mathrm{D}t}\mathbf{V}(\mathbf{r},t), \tag{9}$$

$$-\nabla\times[\nabla\times\mathbf{v}(\mathbf{r},t)] - 2k_2\mathbf{v}(\mathbf{r},t) + k_3\nabla[\nabla\cdot\mathbf{v}(\mathbf{r},t)] + k_2\nabla\times\mathbf{V}(\mathbf{r},t) = R_o\frac{\mathrm{D}}{\mathrm{D}t}\mathbf{v}(\mathbf{r},t), \tag{10}$$

$$\nabla^2\psi(\mathbf{r}) = \frac{m_o^2}{\alpha_o}\sinh[\alpha_o\psi(\mathbf{r})], \tag{11}$$

where

$$\left.\begin{aligned} k_1 &= \frac{\chi}{\mu+\chi}, & k_2 &= \frac{\chi h^2}{\gamma} \\ k_3 &= \frac{\alpha+\beta+\gamma}{\gamma}, & R_e &= \frac{\rho U h}{\mu+\chi} \\ R_o &= \frac{\rho j_o U h}{\gamma}, & m_o &= \frac{h}{\lambda_D} \\ \alpha_o &= \frac{z_o e \psi_o}{k_B T} \end{aligned}\right\}. \tag{12}$$

Here, the parameter k_1 couples the two viscosity coefficients, k_2 and k_3 are normalized micropolar parameters, R_e may be called the Reynolds number, R_o may be called the microrotation Reynolds number (Eringen 2001) and α_o is the ionic-energy parameter (Burgreen and Nakache 1964).

We have already assumed that $\partial/\partial z \equiv 0$; now, we ignore the spatial variations along the x'-axis and set $\partial/\partial x \equiv 0$ consistently with the assumption that $w \gg h$. Furthermore, the one-dimensional flow is supposed to be laminar and symmetric with respect to the y'-axis. Let us therefore designate

$$u = \hat{\mathbf{x}}' \cdot \mathbf{V}, \qquad N = \hat{\mathbf{z}}' \cdot \mathbf{v} \tag{13}$$

for further analysis of non-steady flow in the microchannel. We take the applied electric field to be

$$\mathbf{E}'_{\text{app}}(t') = \hat{\mathbf{x}}' E_o \xi(t' - t_o), \tag{14}$$

such that the switching function

$$\xi(t' - t_o) = \begin{cases} 1, & t' = t_o \\ 0, & t' \neq t_o. \end{cases} \tag{15}$$

Accordingly, equations (8)–(10) reduce to the following system of partial differential equations:

$$\frac{\partial^2}{\partial y^2} u(y,t) + k_1 \frac{\partial}{\partial y} N(y,t) + \frac{\mathrm{d}^2}{\mathrm{d}y^2} \psi(y) \xi(t' - t_o) = R_e \frac{\partial}{\partial t} u(y,t), \tag{16}$$

$$\frac{\partial^2}{\partial y^2} N(y,t) - 2k_2 N(y,t) - k_2 \frac{\partial}{\partial y} u(y,t) = R_o \frac{\partial}{\partial t} N(y,t). \tag{17}$$

As the flow is symmetric—i.e., $u(y,t) = u(-y,t)$ and $\psi(y) = \psi(-y)$—the restrictions

$$\left.\frac{\partial}{\partial y} u(y,t)\right|_{y=0} = 0, \qquad \left.\frac{\mathrm{d}}{\mathrm{d}y} \psi(y)\right|_{y=0} = 0 \tag{18}$$

must hold for all $t > 0$. The boundary conditions on $u(y,t)$ and $\psi(y)$ are (Li 2004, p 95)

$$u(\pm 1, t) = 0, \qquad \psi(\pm 1) = 1, \quad t > 0. \tag{19}$$

In addition, the condition

$$\psi(0) = 0 \tag{20}$$

is engendered by the assumption $h \gg \lambda_D$ (Probstein 1989, p 187). Next, the appropriate initial conditions on $u(y,t)$ and $N(y,t)$ are as follows:

$$u(y,0) = 0, \qquad N(y,0) = 0, \quad y \in [-1,1]. \tag{21}$$

Finally, we impose the boundary conditions

$$N(\pm 1, t) - \beta_o \frac{\partial}{\partial y} u(y,t)\Big|_{y=\pm 1} = 0, \qquad N(0,t) = 0, \quad t > 0, \tag{22}$$

where $\beta_o \in [-1, 0]$ is some constant. As discussed in the predecessor paper (Siddiqui and Lakhtakia 2009), there are two major schools of thought on the boundary condition $(22)_1$. One school ignores microrotation effects near solid walls and sets $\beta_o = 0$ (Eringen 2001, Papautsky *et al* 1999). But the second school holds that $\beta_o < 0$ because the shear and couple stresses on the walls must be high in magnitude in comparison to locations elsewhere, as can be reasoned from the existence of boundary layers (Rees and Bassom 1996, Hegab and Liu 2004). This argument is held valid when thermal transfer and magnetic effects are to be accounted for (Hegab and Liu 2004). In the present case, electric double layers are present; hence, $\beta_o < 0$ may be reasonable if electro-osmosis occurs. Results are provided in this paper for non-zero β_o.

We have shown in the predecessor paper that the electric potential that solves equation (11) and satisfies the boundary conditions $(18)_2$, $(19)_2$ and (20) is

$$\psi(y) = \frac{2}{\alpha_o} \cosh^{-1}\left\{ \frac{1 + \Omega_o \exp[2m_o(|y| - 1)]}{1 - \Omega_o \exp[2m_o(|y| - 1)]} \right\}, \qquad y \in [-1, 1], \tag{23}$$

where

$$\Omega_o = \left| \frac{\cosh(\alpha_o/2) - 1}{\cosh(\alpha_o/2) + 1} \right|. \tag{24}$$

The other variables in equations (16) and (17) remain unknown and have to be determined using a numerical approach.

3. Numerical approach

The interval $y \in [-1, 1]$ was divided into $2I$ segments of size $\Delta y = 1/I$, and J time steps of $\Delta t = 1/J$ were used. We adopted the Du Fort–Frankel scheme which is unconditionally stable as well as accurate to the second order in both space and time (Hoffman 1992, p 683; Thomas 1995, p 302), so that the differential equations (16) and (17) transformed into systems of difference equations. The difference equations were solved iteratively by the successive overrelaxation (SOR) method (Hoffman 1992, p 56). The iterative procedure was repeated until convergence was obtained according to the following criterions (Hoffman 1992, p 425):

$$\max_{i,\,j} \left| \frac{u_{i,j}^{(m+1)} - u_{i,j}^{(m)}}{u_{i,j}^{(m+1)}} \right| < 10^{-5}, \qquad \max_{i,\,j} \left| \frac{N_{i,j}^{(m+1)} - N_{i,j}^{(m)}}{N_{i,j}^{(m+1)}} \right| < 10^{-5}, \tag{25}$$

where $u_{i,j} \equiv u(i\Delta y, j\Delta t)$ and $N_{i,j} \equiv N(i\Delta y, j\Delta t)$, $i \in [0, I]$ and $j \in [0, J]$.

4. Numerical results and discussion

All calculations were made with the following material properties fixed: $n_o = 6.02 \times 10^{22}$ m^{-3}, $z_o = 1$, $\gamma = 10^{-4}$ kg m s^{-1}, $\epsilon = 10\epsilon_o$, $\epsilon_o = 8.854 \times 10^{-12}$ F m^{-1}, $\mu = 3 \times 10^{-2}$ Pa s and $\rho = 1200$ kg m^{-3}. The temperature was fixed at $T = 290$ K. Since the Boltzmann constant $k_B = 1.38 \times 10^{-23}$ J K^{-1} and the electron charge $e = 1.6 \times 10^{-19}$ C, the Debye length $\lambda_D = 10.72$ nm. Consistently with the assumption that $h \gg \lambda_D$, we chose $h \in [536, 5360]$ nm so that $m_o \in [50, 500]$. We used $\psi_o \in \{-500, -100, -25\} \times 10^{-3}$ V. The parameter $k_1 \in [0, 0.95]$ was kept as a variable. The magnitude of the spike of the applied electric field

was fixed at $E_o = 10^4$ V m^{-1}. Moreover, $\Delta y = 1.25 \times 10^{-3}$ and $\Delta t = 2.5 \times 10^{-8}$ were used for calculations.

The dependences of the relevant components of the fluid velocity, microrotation, stress tensor and couple stress tensor on m_o, k_1, β_o and ψ_o were investigated. The fluid velocity and the microrotation have only one non-zero component each: $u'(y', t')$ and $N'(y', t')$, respectively, where $N' = \hat{\mathbf{z}}' \cdot \mathbf{v}'$. The only non-zero components of the stress tensor and the couple stress tensor are (Eringen 2001)

$$\left.\begin{aligned} \sigma'_{12}(y', t') &= \mu \frac{\partial}{\partial y'} u'(y', t') - \chi N'(y', t') \\ \sigma'_{21}(y', t') &= (\mu + \chi) \frac{\partial}{\partial y'} u'(y', t') + \chi N'(y', t') \\ m'_{23}(y', t') &= \gamma \frac{\partial}{\partial y'} N'(y', t') \end{aligned}\right\} . \tag{26}$$

On normalizing the foregoing three quantities, equations (26) take the following form:

$$\left.\begin{aligned} \sigma_{12}(y, t) &= (1 - k_1) \frac{\partial}{\partial y} u(y, t) - k_1 N(y, t) \\ \sigma_{21}(y, t) &= \frac{\partial}{\partial y} u(y, t) + k_1 N(y, t) \\ m_{23}(y, t) &= \frac{\partial}{\partial y} N(y, t) \end{aligned}\right\} . \tag{27}$$

Whereas $\sigma_{12} = \sigma_{21}$ for a simple Newtonian fluid, let us note that the equality does not hold for a micropolar fluid.

4.1. Fluid velocity

We examined the fluid speed $u'(y', t')$ for different values of k_1, β_o and ψ_o, using the numerical approach described in section 3. Some representative results are provided in tables 1 and 2 and figures 1–3 for $\psi_o \in \{-500, -100, -25\} \times 10^{-3}$ V, $m_o = 50$,[3] $k_1 \in \{0, 0.5, 0.95\}$ and $\beta_o \in \{-1, -0.2\}$. The electric-field impulse is applied at time $t_o = 1 \times 10^{-3}$ s.

Figures 1–3 show that the application of the electric-field impulse leads to a surge in the fluid speed, which then decays back to the pre-impulse value. The speed-decay time t'_d is defined by the relation $u'(0, t_o + t'_d) = u'(0, t_o)/2.71828$. Tables 1 and 2 show the speed-decay time for different values of flow and geometric parameters. According to these tables, t'_d

- decreases as k_1 increases for all β_o and ψ_o;
- increases with $|\psi_o|$ for all k_1 and β_o;
- increases as $|\beta_o|$ increases for all k_1 and ψ_o.

Furthermore, t'_d for a simple Newtonian fluid ($k_1 = 0$) is higher than that for a micropolar fluid for all ψ_o.

We found that the fluid speed is maximum midchannel (i.e., at $y' = 0$) for non-steady flow, as also steady flow (Siddiqui & Lakhtakia 2009), due to the no-slip boundary condition $(19)_1$. Accordingly, attention was focused on the variation of $u'(0, t')$ with time t', with some representative results presented in figures 1–3. These figures indicate that the surge in $u'(0, t')$ is instantaneous, upon the application of the electric-field impulse. Furthermore, this

[3] A simple increase in the value of m_o does not change the basic characteristics of all dependences presented in section 4 except that the maximum magnitudes increase. This observation was earlier made for steady flows also (Siddiqui and Lakhtakia (2009).

Table 1. Values of u'_m and t'_d for different values of k_1 and ψ_o, when $m_o = 50$ and $\beta_o = -0.2$.

k_1	ψ_o (V) $\times 10^{-3}$	u'_m (m s^{-1}) $\times 10^{-7}$	t'_d (s) $\times 10^{-9}$
0	−25	7.302	14.924
0.25	−25	12.954	13.945
0.4	−25	14.064	13.481
0.41	−25	14.155	13.452
0.42	−25	14.102	13.427
0.95	−25	2.532	12.649
0	−100	25.379	32.597
0.25	−100	46.441	19.533
0.48	−100	54.756	15.557
0.49	−100	54.801	15.439
0.5	−100	54.732	15.313
0.95	−100	10.146	12.668
0	−500	49.449	154.390
0.25	−500	88.262	111.274
0.64	−500	211.877	27.221
0.65	−500	213.077	25.219
0.66	−500	212.116	23.251
0.95	−500	50.773	12.773

Table 2. Same as table 1 except that $\beta_o = -1$.

k_1	ψ_o (V) $\times 10^{-3}$	u'_m (m s^{-1}) $\times 10^{-7}$	t'_d (s) $\times 10^{-9}$
0.25	−25	52.135	14.217
0.4	−25	78.990	13.810
0.41	−25	79.325	13.783
0.42	−25	80.833	13.759
0.95	−25	103.538	12.697
0.25	−100	179.345	24.109
0.48	−100	343.525	17.321
0.49	−100	351.442	17.206
0.5	−100	362.233	17.075
0.95	−100	418.341	12.870
0.25	−500	352.339	126.195
0.5	−500	952.874	71.771
0.64	−500	1548.562	50.677
0.65	−500	1599.576	48.858
0.66	−500	1656.863	47.237
0.95	−500	2111.223	13.591

maximum value $u'_m = u'(0, t_o)$ of $u'(0, t')$ increases with k_1 for all ψ_o. In addition u'_m also increases as $|\psi_o|$ increases for all k_1 and β_o, which is also clear from the data in tables 1 and 2. The maximum value of u'_m occurs at some $k_1 \neq 0$ for all ψ_o; thus, micropolarity enhances the maximum fluid speed. The value of k_1 which maximizes u'_m increases with $|\psi_o|$ for all β_o.

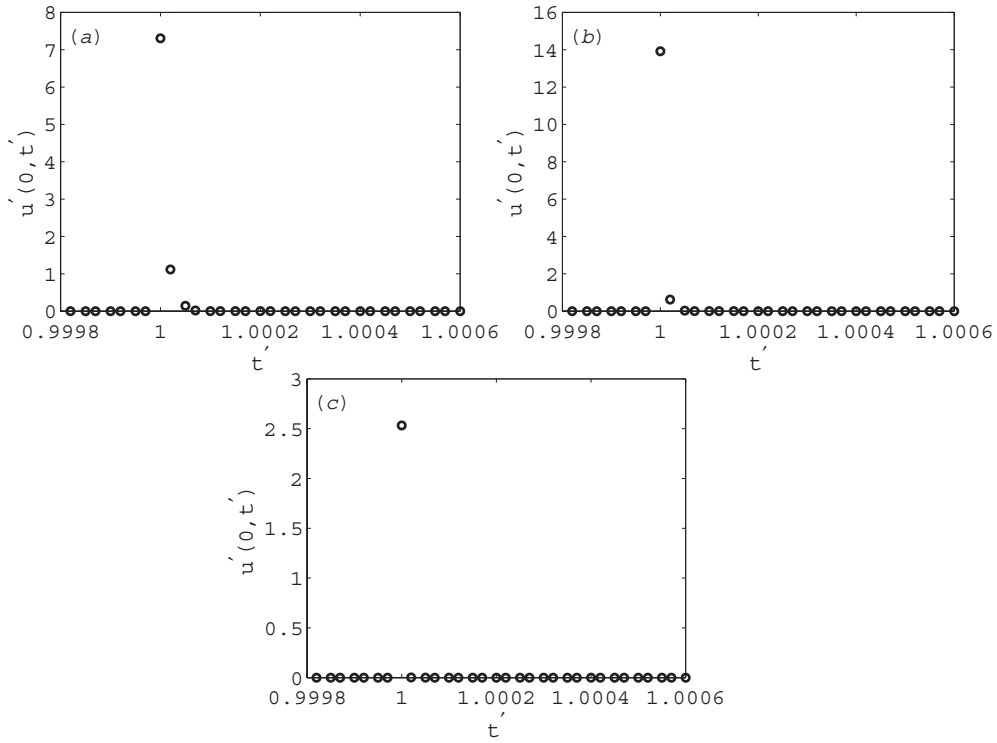

Figure 1. Variation of $u'(0, t')$ ($\times 10^{-7}$ m s^{-1}) with t' ($\times 10^{-3}$ s), when $m_o = 50$, $t_o = 1 \times 10^{-3}$ s, $\beta_o = -0.2$, and $\psi_o = -25 \times 10^{-3}$ V, for (*a*) $k_1 = 0$, (*b*) $k_1 = 0.5$, (*c*) $k_1 = 0.95$.

4.2. Microrotation

The microrotation $N'(y', t')$ is a measure of the spinning speed of the rigid/semi-rigid particles in the fluid about their respective centroids. The chief results pertaining to $N'(y', t_o)$ and $N'(h, t')$ are displayed in figures 4 and 5.

Just like the fluid speed in section 4.1, the microrotation also surges instantaneously upon the application of the electric-field impulse. Figure 4 shows that $|N'(y', t_o)|$ is maximum at the walls $y' = \pm h$ and is null-valued at the centre $y' = 0$ of the microchannel. Both conclusions are in agreement with conditions (22), and had been obtained for steady flow also (Siddiqui & Lakhtakia 2009). Moreover, this figure reveals that $|N'(y', t_o)|$

- decreases as k_1 increases for all β_o and ψ_o;
- decreases as $|\psi_o|$ increases for all k_1 and β_o;
- increases as $|\beta_o|$ increases for all k_1 and ψ_o.

Table 3 contains data on τ'_d, the microrotation-decay time defined by the relation $N'(h, t_o + \tau'_d) = N'(h, t_o)/2.71828$, and $N'_m = |N'(\pm h, t_o)|$, the maximum magnitude of the microrotation in the microchannel. This table indicates that the microrotation-decay time

- decreases as k_1 increases for all β_o and ψ_o;
- increases as $|\psi_o|$ increases for all k_1 and β_o;
- increases as $|\beta_o|$ increases for all k_1 and ψ_o.

Consequently, we surmise that τ'_d is proportional to t'_d.

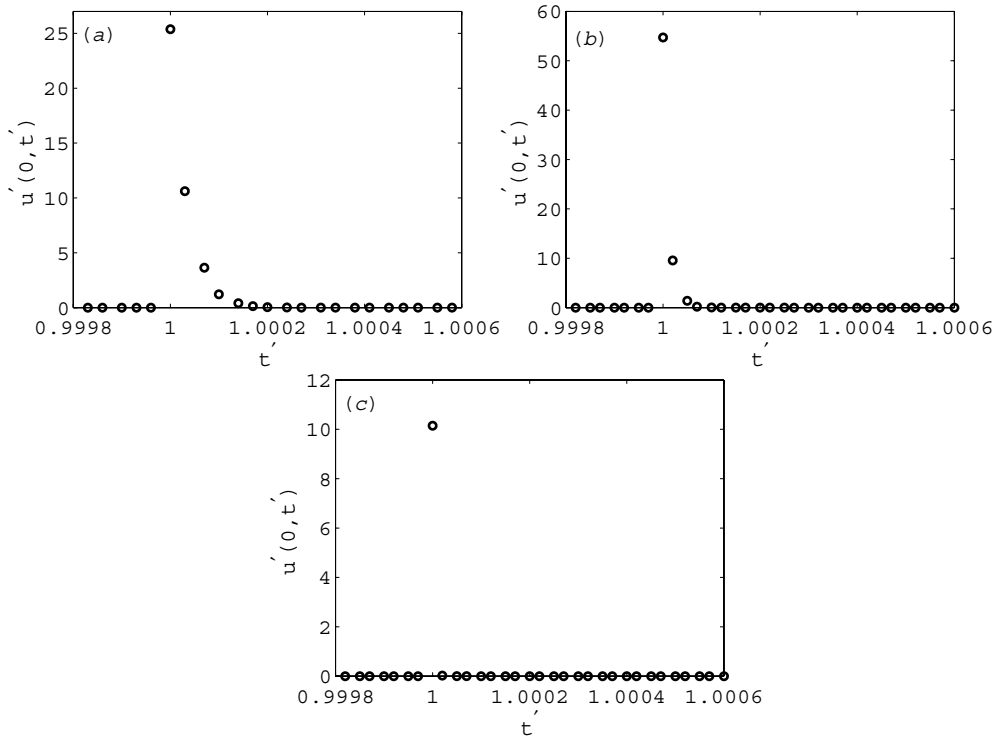

Figure 2. Same as figure 1, except that $\psi_o = -100 \times 10^{-3}$ V.

Table 3. Values of N'_m and τ'_d for different values of k_1, β_o and ψ_o, when $m_o = 50$.

k_1	β_o	ψ_o (V) $\times 10^{-3}$	N'_m (s^{-1})	τ'_d (s) $\times 10^{-9}$
0.25	−0.2	−25	10.938	12.726
0.95	−0.2	−25	0.854	12.643
0.25	−0.2	−100	217.212	12.935
0.95	−0.2	−100	17.135	12.646
0.25	−0.2	−500	309.390	13.080
0.95	−0.2	−500	27.093	12.662
0.25	−1	−25	69.275	12.942
0.95	−1	−25	43.362	12.690
0.25	−1	−100	268.769	13.648
0.95	−1	−100	175.105	12.838
0.25	−1	−500	1188.424	13.837
0.95	−1	−500	882.230	13.457

Table 3 also lets us conclude that the maximum magnitude N'_m of the microrotation decreases as k_1 increases for all ψ_o and β_o; it also decreases as $|\psi_o|$ increases for all k_1 and β_o. Figure 5 showing the variation of $N'(h, t')$ with t' is in agreement with these conclusions.

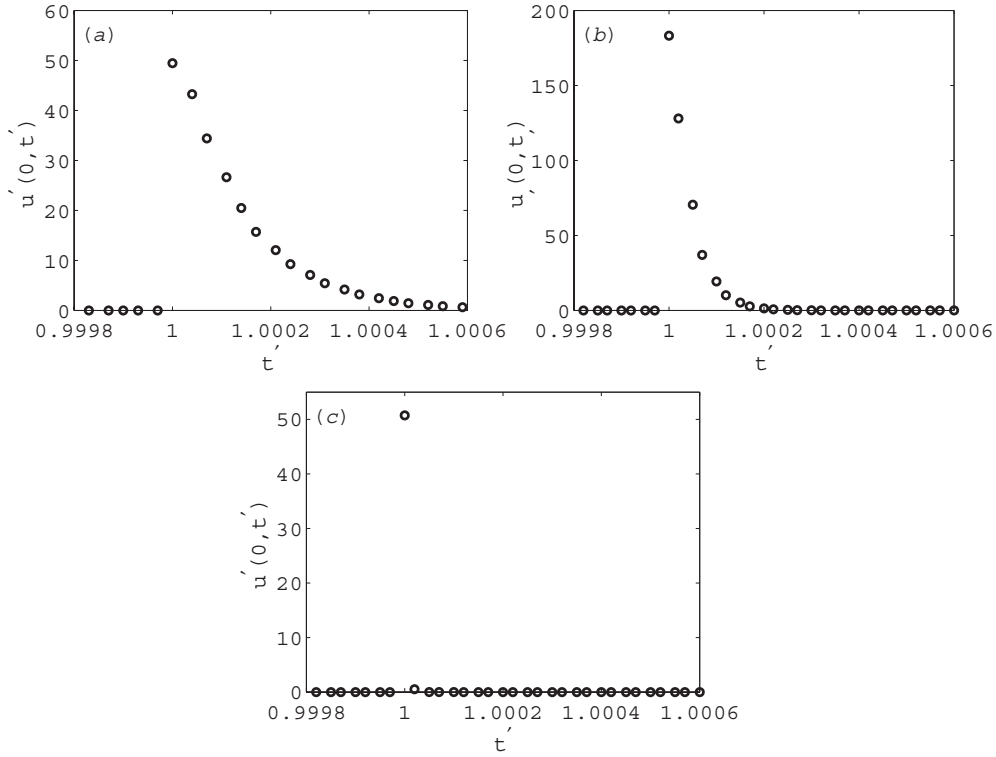

Figure 3. Same as figure 1, except that $\psi_o = -500 \times 10^{-3}$ V.

4.3. Stress tensor

Like $N'(y', t')$, the component $\sigma'_{12}(y', t') = -\sigma'_{12}(-y', t')$ of the stress tensor is maximum in magnitude at the two walls but is absent at the centre of the microchannel. In addition, its temporal profile shows that $\sigma'_{12}(y', t')$ attains its maximum value at $t' = t_o$. These results are exemplified by figures 6 and 7.

The spatial profiles of $\sigma'_{12}(y', t_o)$ in figure 6 reveal that the maximum magnitude $\sigma'_{12_m} = |\sigma'_{12}(\pm h, t_o)|$ of $\sigma'_{12}(y', t_o)$ decreases as k_1 increases for low values of k_1 for all low value of $|\beta_o|$. However, this magnitude increases as k_1 increases for higher values of k_1 for all low values of $|\beta_o|$. Moreover, σ'_{12_m} increases with $|\beta_o|$ for all k_1 and ψ_o, and it also intensifies with increasing $|\psi_o|$ for all k_1 and β_o. Both of these results are exemplified by figure 7.

Analogous to the component $\sigma'_{12}(y', t')$ of the stress tensor, the component $\sigma'_{21}(y', t')$ is dominant at the walls of microchannel and also adheres to the spatial symmetry $\sigma'_{21}(y', t') = -\sigma'_{21}(-y', t')$. In addition, the increasing/decreasing trend of $\sigma'_{21}(y', t')$ is the same as that of $\sigma'_{12}(y', t')$ with respect to y', t', k_1, β_o and ψ_o. However, $|\sigma'_{21}(y', t')|$ exceeds $|\sigma'_{12}(y', t')|$ at the walls of the microchannel. We decided not to illustrate these results here.

4.4. Couple stress tensor

The couple stress tensor appears, in addition to the usual (Cauchy) stress tensor, in micropolar fluids as it is generated by the rotational degrees of freedom of the rigid/semi-rigid particles

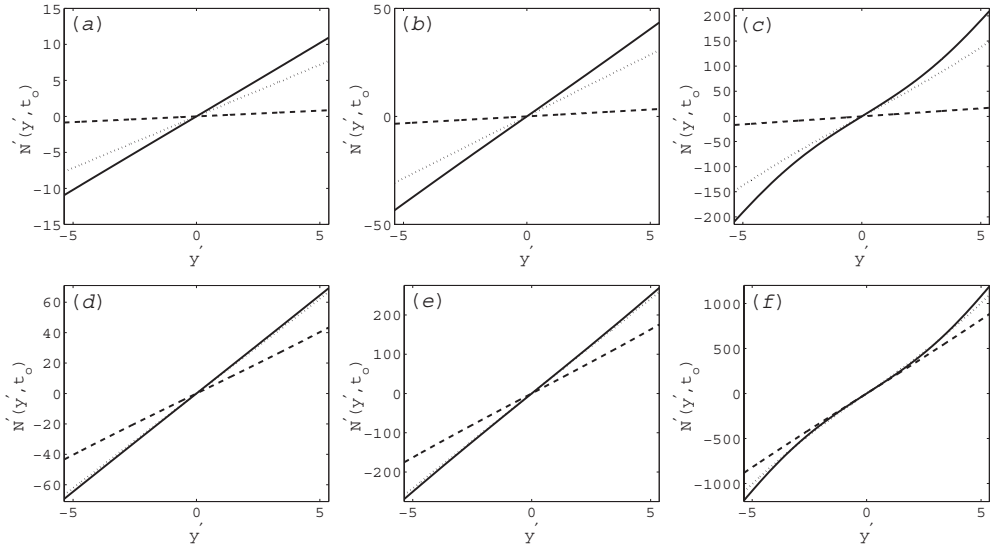

Figure 4. Variation of $N'(y', t_o)$ (s^{-1}) with y' ($\times 10^{-7}$ m) when $m_o = 50$, for $k_1 = 0.25$ (solid curves), $k_1 = 0.5$ (dotted curves), $k_1 = 0.95$ (dashed curves). (*a*)–(*c*) $\beta_o = -0.2$ and (*d*)–(*f*) $\beta_o = -1$. (*a*), (*d*) $\psi_o = -25 \times 10^{-3}$ V, (*b*), (*e*) $\psi_o = -100 \times 10^{-3}$ V and (*c*), (*f*) $\psi_o = -500 \times 10^{-3}$ V.

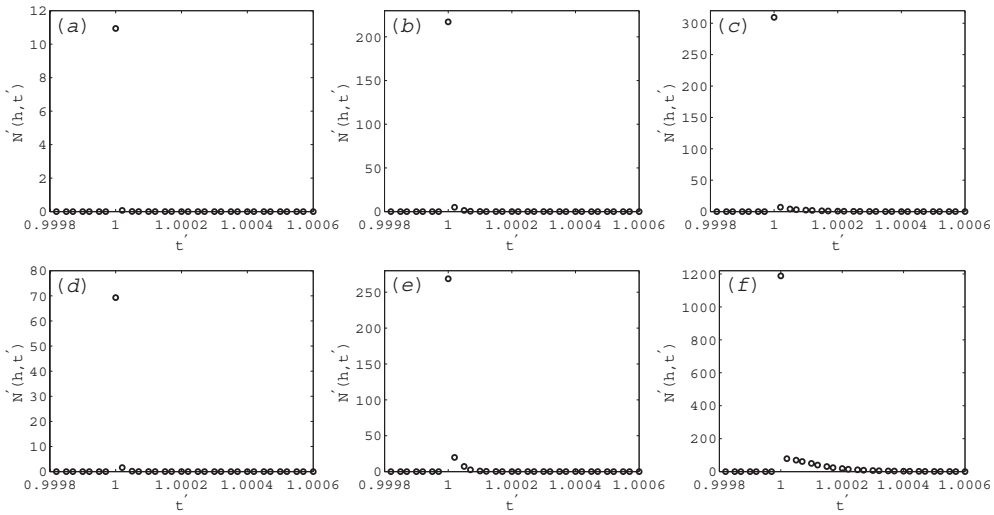

Figure 5. Variation of $N'(h, t')$ (s^{-1}) with t' ($\times 10^{-3}$ s), when $k_1 = 0.25$ and $m_o = 50$. (*a*)–(*c*) $\beta_o = -0.2$ and (*d*)–(*f*) $\beta_o = -1$. (*a*), (*d*) $\psi_o = -25 \times 10^{-3}$ V, (*b*), (*e*) $\psi_o = -100 \times 10^{-3}$ V and (*c*), (*f*) $\psi_o = -500 \times 10^{-3}$ V.

therein. Just like all other quantities examined thus far in this section, the only non-zero component of the couple stress tensor also surges instantaneously in response to the application of the electric-field impulse. Its temporal profiles show that it achieves its maximum values at $t' = t_o$.

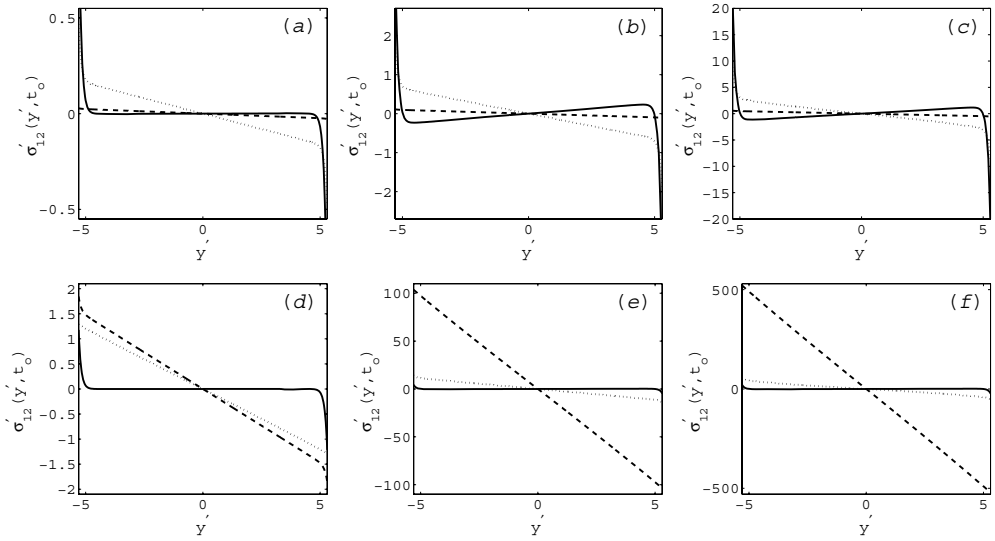

Figure 6. Variation of $\sigma'_{12}(y', t_o)$ (N m^{-1}) with y' ($\times 10^{-7}$ m) when $m_o = 50$, for $k_1 = 0$ (solid curves), $k_1 = 0.5$ (dotted curves), $k_1 = 0.95$ (dashed curves). (*a*)–(*c*) $\beta_o = -0.2$ and (*d*)–(*f*) $\beta_o = -1$. (*a*), (*d*) $\psi_o = -25 \times 10^{-3}$ V, (*b*), (*e*) $\psi_o = -100 \times 10^{-3}$ V and (*c*), (*f*) $\psi_o = -500 \times 10^{-3}$ V.

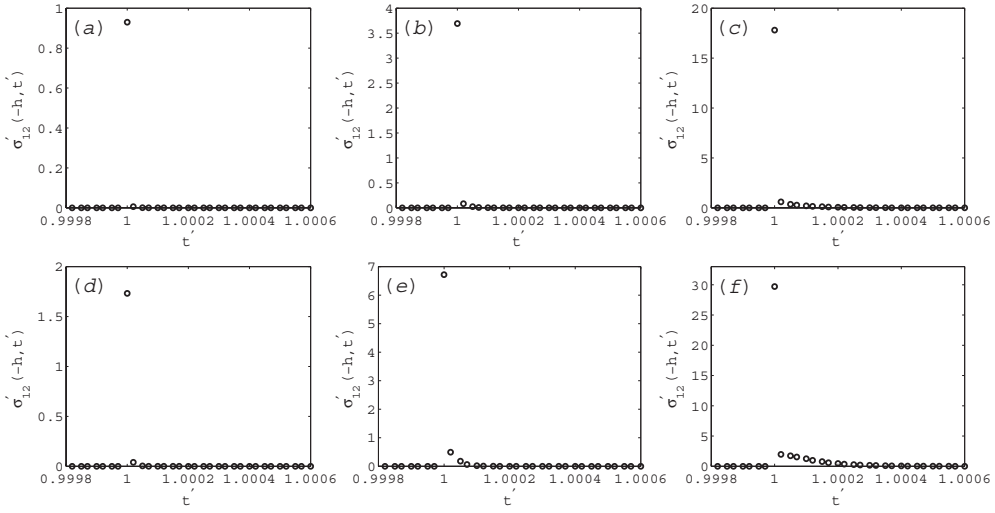

Figure 7. Variation of $\sigma'_{12}(-h, t')$ (N m^{-1}) with t' ($\times 10^{-3}$ s), when $k_1 = 0.25$ and $m_o = 50$. (*a*)–(*c*) $\beta_o = -0.2$ and (*d*)–(*f*) $\beta_o = -1$. (*a*), (*d*) $\psi_o = -25 \times 10^{-3}$ V, (*b*), (*e*) $\psi_o = -100 \times 10^{-3}$ V and (*c*), (*f*) $\psi_o = -500 \times 10^{-3}$ V.

Figure 8 represents the variation of $m'_{23}(y', t_o)$ with y'. It shows that $m'_{23}(y', t_o)$ is independent of y' for $|\psi_o| < 100 \times 10^{-3}$ V for all k_1 and β_o, but not when $|\psi_o| \geqslant 100 \times 10^{-3}$ V. Furthermore, $m'_{23}(y', t_o)$

- increases as $|\psi_o|$ increases for all k_1 and β_o;

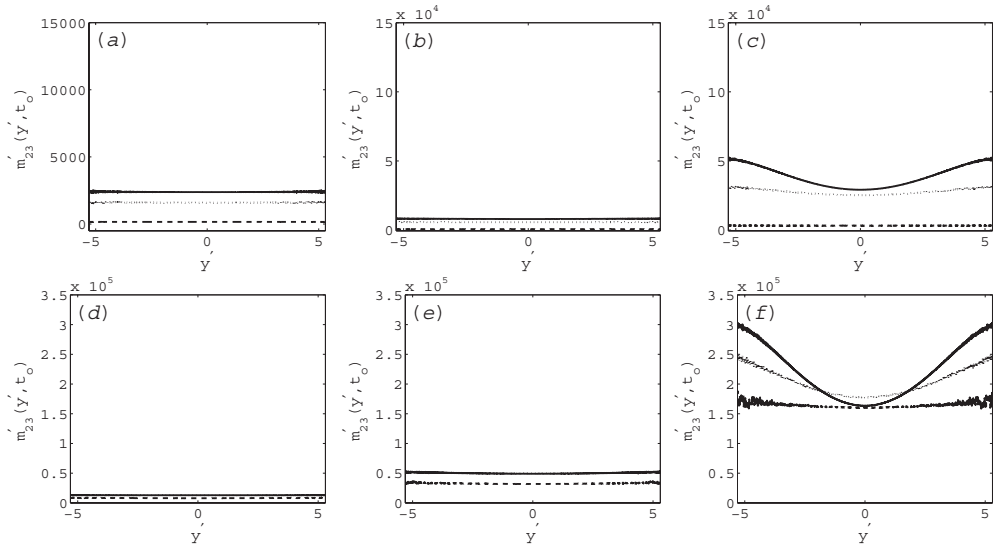

Figure 8. Variation of $m'_{23}(y', t_o)$ ($\mathrm{m}^{-1}\ \mathrm{s}^{-1}$) with y' ($\times 10^{-7}$ m) when $m_o = 50$, for $k_1 = 0.25$ (solid curves), $k_1 = 0.5$ (dotted curves), $k_1 = 0.95$ (dashed curves). (*a*)–(*c*) $\beta_o = -0.2$ and (*d*)–(*f*) $\beta_o = -1$. (*a*), (*d*) $\psi_o = -25 \times 10^{-3}$ V, (*b*), (*e*) $\psi_o = -100 \times 10^{-3}$ V and (*c*), (*f*) $\psi_o = -500 \times 10^{-3}$ V.

- increases as $|\beta_o|$ increases for all k_1 and ψ_o;
- decreases as k_1 increases for all β_o and ψ_o.

Of course, $m'_{23}(y', t') \equiv 0$ when micropolarity is absent ($k_1 = 0$).

5. Concluding remarks

We formulated the initial-boundary-value problem of non-steady electro-osmotic flow of a micropolar fluid in a rectangular microchannel, provided that the Debye length is no more than 5% of the height of the microchannel and the length of the microchannel is much larger than its height. The governing differential equations were solved numerically using the Du Fort–Frankel scheme, when a spatially uniform electric field is applied as an impulse of finite magnitude. The effect of this impulse is instantaneous in the temporal profiles of the fluid speed, microrotation, stress and couple stress—for micropolar as well as simple Newtonian fluids.

Numerical results showed that the fluid speed depends significantly on the micropolar nature of the fluid as expressed through a boundary parameter (β_o) that mediates the velocity gradient and the microrotation at the walls of the microchannel and a viscosity coupling parameter (k_1) relating the Newtonian shear viscosity coefficient and the (micropolar) vortex viscosity coefficient—in agreement with the results for steady flow examined in Siddiqui and Lakhtakia (2009). Furthermore, the decay time of the fluid speed intensifies with the increase in the magnitudes of $|\beta_o|$ and the zeta potential $|\psi_o|$. Notably however, it decreases if the micropolarity (i.e., $k_1 \neq 0$) is increased. Furthermore, the decay time of fluid speed for a micropolar fluid is less than for a comparable simple Newtonian fluid.

The fluid speed is dominant midchannel but null-valued at the walls, this trend being just the opposite for the microrotation. Moreover, the maximum magnitude of microrotation intensifies with increasing magnitude of the zeta potential, but it decreases as the viscosity coupling parameter increases. The microrotation-decay time appears to be proportional to the speed-decay time.

Although the stress tensor is dependent on both fluid speed and microrotation, the effect of microrotation is more dominant than that of the fluid speed. An increase in the magnitude of either the zeta potential or the boundary parameter enhances the magnitude of the stress components at the walls of the microchannel. A threshold effect is evident in the spatial profile of the couple stress tensor: it is spatially uniform for $|\psi_o|$ less than a certain value (100 mV for the chosen parameters) but varies spatially for a zeta potential of higher magnitude.

Given that the effect of the application of the electric-field impulse is instantaneous in the temporal profiles of the fluid speed, microrotation, stress and couple stress, we expect similar trends even when the applied electric field varies over some finite interval of time. Therefore, analysis for non-steady flows can be adequately substituted by the simpler analysis for steady flow.

Acknowledgments

AAS is grateful to the Higher Education Commission of Pakistan for a grant to enable him to visit Penn State. AL thanks the Charles Godfrey Binder Endowment at Penn State for partial financial support.

References

Ahmadi G 1976 Self similar solution of incompressible micropolar boundary layers flow over a semi-infinite plate *Int. J. Eng. Sci.* **14** 639–46

Arangoa M A, Campanero M A, Popineau Y and Irache J M 1999 Electrophoretic separation and characterization of gliadin fractions from isolates and nanoparticulate drug delivery systems *Chromatographia* **50** 243–6

Ariman T, Turk M A and Sylvester N D 1973 Microcontinuum fluid mechanics—a review *Int. J. Eng. Sci.* **11** 905–30

Burgreen D and Nakache F R 1964 Electrokinetic flow in ultrafine capillary slits *J. Phys. Chem.* **68** 1084–91

Eijkel J C T and van den Berg A 2006 The promise of nanotechnology for separation devices—from a top-down approach to nature-inspired separation devices *Electrophoresis* **27** 677–85

Eringen A C 1973 On nonlocal microfluid mechanics *Int. J. Eng. Sci.* **11** 291–306

Eringen A C 2001 *Microcontinuum Field Theories, vol 2: Fluent Media* (New York: Springer)

Fluri K, Fitzpatrick G, Chiem N and Harrison D J 1996 Integrated capillary electrophoresis devices with an efficient postcolumn reactor in planar quartz and glass chips *Anal. Chem.* **68** 4285–90

Hegab H E and Liu G 2004 Fluid flow modeling of micro–orifices using micropolar fluid theory *Proc. SPIE* **4177** 257–67

Hoffman J D 1992 *Numerical Methods for Engineers and Scientists* (New York: McGraw-Hill)

Li D 2004 *Electrokinetics in Microfluidics* vol 2 (London: Elsevier)

Misra J C and Ghosh S K 2001 A mathematical model for the study of interstitial fluid movement vis-à-vis the non-Newtonian behaviour of blood in a constricted artery *Comput. Math. Appl.* **41** 783–811

Papautsky I, Brazzle J, Ameel T and Frazier A B 1999 Laminar fluid behavior in microchannel using micropolar fluid theory *Sensors Actuators* A **73** 101–8

Probstein R F 1989 *Physicochemical Hydrodynamics: An Introduction* (Stoneham, MA: Butterworths)

Rees D A S and Bassom A P 1996 The Blasius boundary-layer flow of a micropolar fluid *Int. J. Eng. Sci.* **34** 113–24

Riehemann K, Schneider S W, Luger T A, Godin B, Ferrari M and Fuchs H 2009 Nanomedicine—challenges and perspectives *Angew. Chem. Int. Ed.* **48** 872–97

Siddiqui A A and Lakhtakia A 2009 Steady electro-osmotic flow of a micropolar fluid in a microchannel *Proc. R. Soc. Lond.* A **465** 501–22

Thomas J W 1995 *Numerical Partial Differential Equations: Finite Difference Methods* (New York: Springer)

Turk M A, Sylvester N D and Ariman T 1973 On pulsatile blood flow *J. Rheol.* **17** 1–21